CrossMark

ORIGINAL PAPER

Dichroism in the Parent Ferropnictide BaFe$_2$As$_2$ Across the Nematic Phase Transition

M. Chinotti[1] · C. Mirri[1] · A. Dusza[1] · S. Bastelberger[1] · L. Degiorgi[1] · J.-H. Chu[2,3,4] · H.-H. Kuo[2,3,4] · I. R. Fisher[2,3,4]

Abstract We investigate the anisotropy of the optical response (i.e., dichroism) in the representative 'parent' ferropnictide BaFe$_2$As$_2$. The dichroism is achieved through measurements of the optical reflectivity in a broad spectral range, across the tetragonal-to-orthorhombic and spin-density-wave (SDW) phase transitions, from which we extract the real part of the optical conductivity. The collection of data on the specimen with variable degree of detwinning is made possible via our novel pressure device which allows tuning in situ uniaxial stress. The dichroism bears testimony to an important electronic polarization, reflecting the impact of the nematic phase and its fluctuations on the electronic structure.

✉ L. Degiorgi
degiorgi@solid.phys.ethz.ch

1 Laboratorium für Festkörperphysik, ETH - Zürich, 8093 Zürich, Switzerland

2 Geballe Laboratory for Advanced Materials, Department of Applied Physics, Stanford University, Stanford CA 94305, USA

3 Stanford Institute for Materials and Energy Sciences, Stanford University, Stanford CA 94305, USA

4 SLAC National Accelerator Laboratory, 2575 Sand Hill Road, Menlo Park CA 94025, USA

The ferropnictides harbor a structural tetragonal-to-orthorhombic transition at a temperature T_s that may either be coincident with or precede a transition into a long-range antiferromagnetic order (AFM) at T_N, usually ascribed to a spin-density-wave (SDW) state. All measurable physical quantities thus suffer a twofold in-plane anisotropy, directly imaging the development of symmetry-breaking states and implying the onset of an electronic nematic phase [1, 2]. In order to minimize the elastic energy, dense structural twins form at $T < T_s$, which mask the anticipated in-plane anisotropy of measurable physical quantities in the orthorhombic phase. Such an anisotropy can be recovered by aligning the domains along a preferential direction (i.e., by detwinning the specimens), which may be achieved in large magnetic fields or by exerting uniaxial stress [1–7]. We recently developed a technique using a gas-bellows to tune the uniaxial stress that is exerted on samples, which is well suited to the temperature regime below as well as across T_s [8, 9].

Our previous work pointed out the remarkable fingerprint of the nematic state at energy scales far away from the Fermi level, therefore pertinent to the electronic structure [8, 9]. The focus of the present work is on the overall anisotropy of the complete optical response. We investigate the in-plane optical conductivity of the parent compound BaFe$_2$As$_2$ beyond the mid-infrared (MIR) interval studied so far, covering the spectral range from the far infrared (FIR) to the ultraviolet (UV), at several combinations of temperature and in situ tunable uniaxial pressure. Our goal is to probe the anisotropy of the optical conductivity, from which we can define the linear dichroism. Our optical measurement is thus an excellent probe in order to study the impact of the nematic phase on the charge dynamics and electronic properties, since it spans a vast energy interval, extending from the Fermi surface (FS) to energies deep into the electronic structure.

The reflectivity $R(\omega)$ was measured on as-grown $BaFe_2As_2$ single crystal at nearly normal incidence [10] with the electromagnetic radiation polarized along the crystallographic axes. The structural and SDW transition occur at $T_s = T_N = 135$ K (from now on denoted as $T_{s,N}$). The specimen was mounted into the pressure device, described in Refs. [8] and [9], which consists of a spring bellows connected through a capillary to a pipeline outside the cryostat. The bellows can be extended/retracted by flushing He gas into its volume or evacuating it through the pipeline, thus exerting and releasing uniaxial pressure on the lateral side of the specimen (see Fig. 1 of Ref. [9]). The uniaxial pressure, detwinning the samples, is thus applied parallel to the b axis, which is preferentially aligned along the direction of a compressive stress and corresponds to the shorted orthorhombic ferromagnetic axis. We refer to the He-gas pressure inside the volume of the bellows: the effective pressure felt by the sample depends on its size and thickness, so that a He gas pressure of 0.1 bar on our $BaFe_2As_2$ crystal means an effective pressure of about 1.5 MPa. Here, we report results obtained from the so-called zero-pressure-cooled (ZPC) experiment. From above $T_{s,N}$ we cool down the sample to the selected temperature (T), without applying any pressure (p). At that T, kept fixed during the whole experiment, we progressively increase p in step of 0.2 bar from 0 to a maximum pressure of 0.8 bar and measure $R(\omega)$ in the energy interval $\omega \sim 60$ to 7000 cm^{-1} at each step. Then, we complete the 'pressure loop' by measuring $R(\omega)$ when releasing p back to 0 bar. These data were complemented with measurements at 300 K up to 40,000 cm^{-1} for unstressed crystals. The optical conductivity was finally extracted from the reflectivity spectrum through Kramers-Kronig (KK) transformations, making use of appropriate extrapolations [10]. Further details about the experimental technique and setup can be found in Refs. [8–11].

Figure 1 displays the real part $\sigma_1(\omega)$ of the optical conductivity. The upper right panel (a) emphasizes the temperature dependence of $\sigma_1(\omega)$ for the unstressed (twinned) specimen, in overall good agreement with our previous results [12]. At $T \geq T_{s,N}$, $\sigma_1(\omega)$ is weakly temperature dependent, tending to a constant value in the FIR range, as it is common for a conducting material. Below $T_{s,N}$, the transition into the long-range AFM state opens a partial-gap, which depletes $\sigma_1(\omega)$ in FIR below 1000 cm^{-1} and, due to the reshuffled spectral weight, leads to an enhancement at MIR frequencies, forming a peak centered at about 1300 cm^{-1}. The un-gapped portion of FS contributes to the metallic response of $\sigma_1(\omega)$ finally merging into a narrow zero-energy mode below 200 cm^{-1}. The temperature dependence of $\sigma_1(\omega)$ expires above 3000 cm^{-1} at the onset of the absorption peaked around 7000 cm^{-1} and attributed to electronic interband transitions [13, 14].

The color maps of Fig. 1b–m reproduce the p dependence of $\sigma_1(\omega)$ in the FIR-MIR spectral range ($\omega \sim 60$–2500 cm^{-1}) at selected temperatures above, at and below $T_{s,N}$ for both polarization directions. The lower the temperature, the stronger is the optical anisotropy achieved upon applying uniaxial stress. Along the elongated orthorhombic antiferromagnetic a axis, the depletion of $\sigma_1(\omega)$ in FIR becomes less pronounced, the intensity of the MIR absorption increases and its peak frequency shifts to lower energy upon increasing p. Quite the opposite behavior is observed along the b axis (see, e.g., Fig. 1l and m). The right panels (n–s) of Fig. 1 emphasize the T dependence of the optical response for selected p (i.e., at $p = 0$ bar, at saturation for $p = 0.8$ bar and at released 0 bar pressure). The resulting optical anisotropy saturates at 0.8 bar for $T \ll T_{s,N}$. The enhancement of the MIR absorption feature at about 1300 cm^{-1} is clearly evident, primarily along the a axis, as well as the stronger depletion of $\sigma_1(\omega)$ at $\omega < 1000$ cm^{-1} along the b axis with decreasing temperature below $T_{s,N}$ (Fig. 1p and q). Additionally, we remark the low temperature narrowing of $\sigma_1(\omega)$ at $\omega < 300$ cm^{-1} (Fig. 1l, m, p and q), which is more pronounced along the b axis. Upon releasing the compressive stress back to zero, a remanent anisotropy still persists at temperatures $T < T_{s,N}$ (Fig. 1l, m, r and s), but it fully collapses at $T \cong T_{s,N}$ (Fig. 1f, g, r and s). In other words, we can be certain that the orthorhombic state is strongly anisotropic even in the absence of any external strain. The p-dependent optical anisotropy at $T \leq T_s$ is thus reminiscent of a hysteretic behavior [8, 9], which is consistent with earlier magnetoresistance measurements using an in-plane magnetic field to partially detwin single crystal samples [1, 3]. Moreover, the weakly p-dependent stress-induced anisotropy in $\sigma_1(\omega)$ for $T > T_s$ is observable for temperatures up to at least 160 K for $p \geq 0.4$ bar and is reversible upon sweeping p (Fig. 1d–g). Overall, one can safely state that at low T and for the single domain-like specimen $\sigma_1(\omega)$ is more enhanced along the a axis with respect to the b axis for $\omega \leq 2000$ cm^{-1}.

In order to emphasize the evolution of the optical anisotropy, we calculate the quantity $\Delta\sigma_1(\omega, p; T) = \sigma_1^a(\omega, p; T) - \sigma_1^b(\omega, p; T)$, which represents the optical dichroism. Panels (a–e) in Fig. 2 display the p dependence of $\Delta\sigma_1(\omega, p; T)$ at selected T. The panels (f–l) in Fig. 2 convey the evolution of the dichroism at saturation (i.e., at 0.8 bar) upon lowering the temperature across $T_{s,N}$. The largest dichroism at saturation occurs at $T \ll T_{s,N}$, as clearly emphasized in Fig. 2l. Figure 3 shows alternatively $\Delta\sigma_1(\omega, T; p)$ as a function of T at fixed p of 0 bar, 0.8 bar and released 0 bar.

Figures 2 and 3 further highlight the features pointed out above, when qualitatively sketching the major findings evinced from the rough data of Fig. 1. All
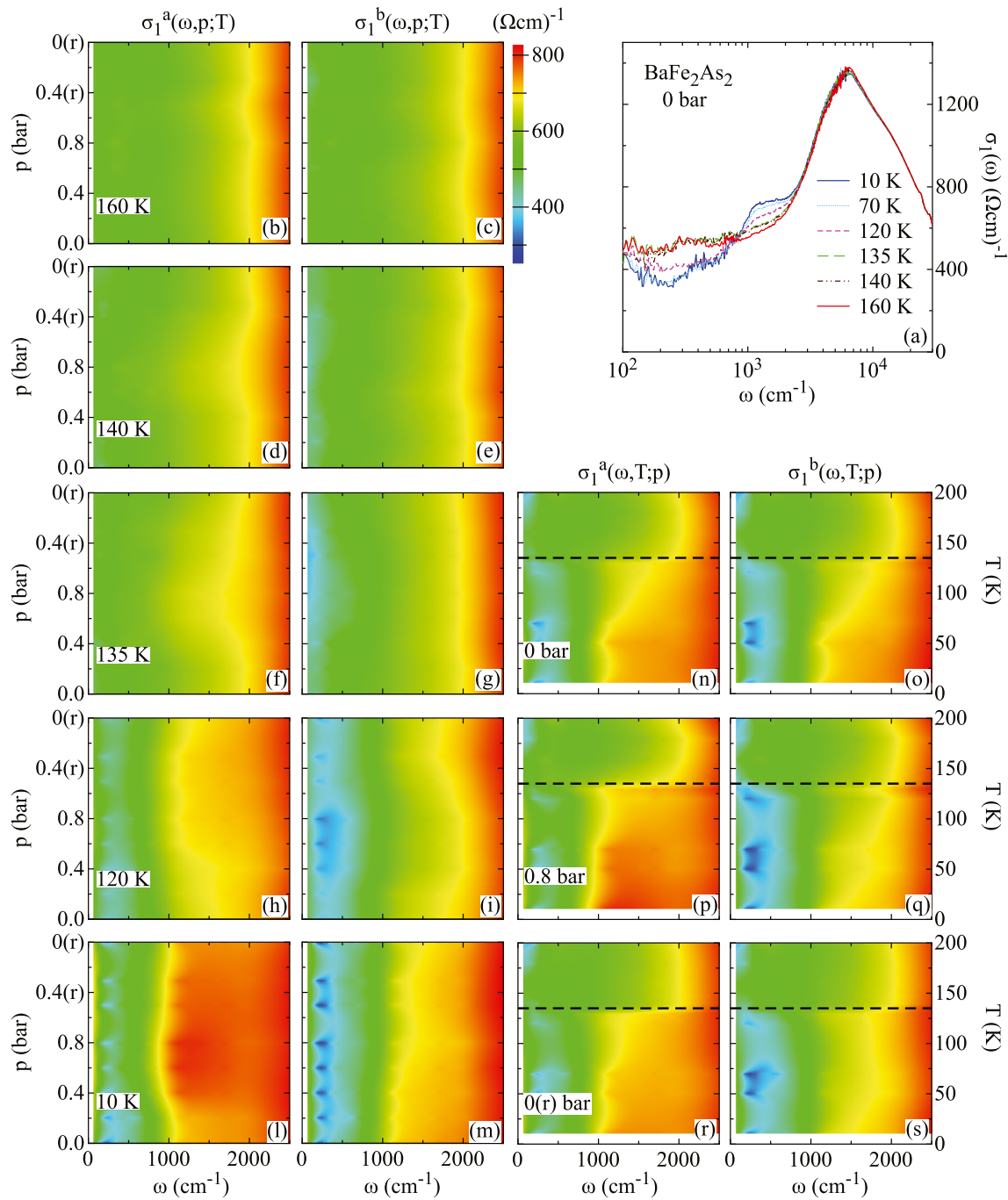
Fig. 1 The *upper right* panel (**a**) shows the temperature dependence of $\sigma_1(\omega)$ in the FIR-UV range (in a semi-log scale) at 0 bar (i.e., twinned sample) [11]. The *color maps* (**b–m**) display the pressure dependence of the real part $\sigma_1(\omega)$ of the optical conductivity up to 2500 cm^{-1} along the *a* and *b* axis at selected temperatures: **b**, **c** 160 K; **d**, **e** 140 K; **f**,**g** 135 K; **h**, **i** 120 and **l**, **m** 10 K [11]. The temperature dependence (**n–s**) of the in-plane optical conductivity up to 2500 cm^{-1} along both axes of BaFe$_2$As$_2$ is also shown at the selected uniaxial pressures: **n–o** 0 bar, **p–q** 0.8 bar, and **r–s** released 0 bar. Data have been interpolated using a first-neighbor interpolation procedure to generate the color maps. Released pressures are denoted by '(r)'. The *color scale* applies to all maps. The *dashed line* indicates the transition temperature $T_{s,N}$

characteristic fingerprints of the optical anisotropy are particularly evident for the fully detwinned specimen (Fig. 2f–l). The optical anisotropy undergoes a smooth but progressive enhancement in the FIR-MIR spectral range (i.e., for $\omega \leq 2000$ cm^{-1}) when lowering T. Such an anisotropy indicates that the nematic phase influences the electronic structure of the title compound differently between the two axes. There is overall more spectral weight which accumulates along the *a* axis than along the *b* axis for frequencies up to the MIR range. Upon crossing $T_{s,N}$, one may observe,

Fig. 2 The color maps display the pressure dependence of the optical dichroism $\Delta\sigma_1(\omega, p; T) = \sigma_1^a(\omega, p; T) - \sigma_1^b(\omega, p; T)$ up to 2500 cm^{-1} at **a** 160 K, **b** 140 K, **c** 135 K, **d** 120, and **e** 10 K. Data have been interpolated using a first-neighbor interpolation procedure to generate the color maps. Released pressures are denoted by '(r)'. Panels (**f–l**) show $\Delta\sigma_1(\omega, p; T)$ at selected T and at fixed $p = 0.8$ bar (i.e., at saturation)
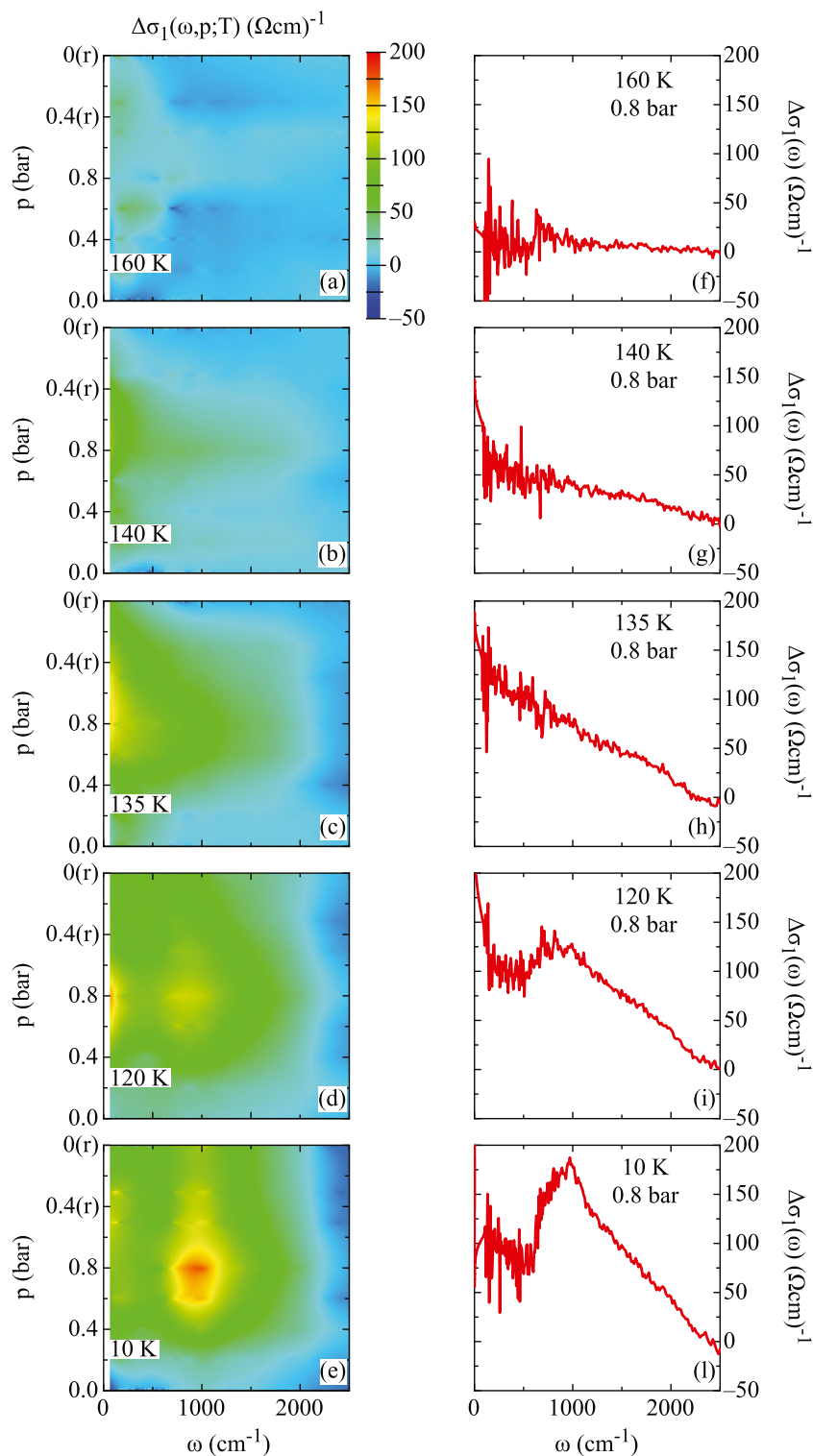
besides the anisotropy in the effective metallic (Drude) part of $\Delta\sigma_1(\omega \rightarrow 0)$, the appearance of a prominent anisotropic peak in $\Delta\sigma_1(\omega)$ at 1000 cm^{-1}. This bears testimony that the nematic phase also affects energy scales deep into the electronic structure, thus far away from the Fermi energy. Figures 2 and 3 iterate again that the dichroism achieved at

saturation (i.e., $p = 0.8$ bar) persists at $T \leq T_{s,N}$ and is fully reversible at $T > T_{s,N}$ upon releasing p.

One of the major debated issues is about the role played by orbital and magnetic order, spin fluctuations, and impurity scattering in defining the underlying physics of this class of materials, particularly in terms of their anisotropic
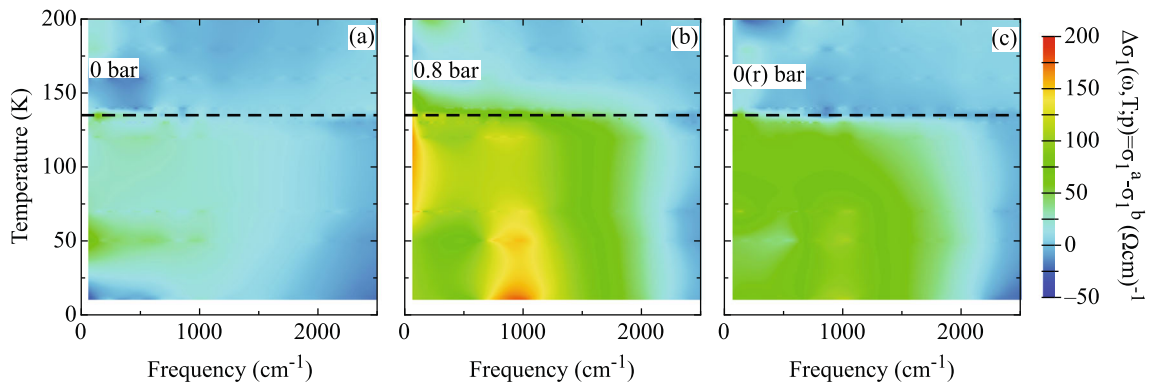
Fig. 3 Color maps of the temperature dependence of $\Delta\sigma_1(\omega, T; p) = \sigma_1^a(\omega, T; p) - \sigma_1^b(\omega, T; p)$ up to 2500 cm^{-1} at **a** 0 bar, **b** 0.8 bar, and **c** released 0 bar (r). Data have been interpolated using a first-neighbor interpolation procedure to generate the color maps. The *dashed line* indicates the transition temperature $T_{s,N}$

physical properties. We start our theoretical (yet not comprehensive) survey by quoting the calculation of the X-ray absorption linear dichroism by Chen et al. [15], who first anticipated the importance of orbital order. The orbital order is represented by an energy splitting between the two otherwise degenerate d_{xz} and d_{yz} orbitals. They show that the FS reconstruction below T_N, as evinced in angle-resolved photoemission spectroscopy experiments [16, 17], may be understood when the SDW field is further accompanied by an orbital polarization, consistent with the dichroism shown in Fig. 2. The optical conductivity was then explicitly calculated by Lv and Phillips [18], within the five-orbital Hubbard model using a self-consistent mean-field theory. They state that the inclusion of both orbital and magnetic order is essential. Such an orbital nematic order is well imaged by the optical anisotropy discovered at MIR frequencies (Figs. 2 and 3). Furthermore, the magnetic order theoretically leads to the reshuffling of spectral weight at low T, which induces the enhancement/depletion of $\sigma_1(\omega)$ in its metallic part along the a/b axis, respectively, the opening of a partial gap as well as the emergence of anisotropic peaks in $\sigma_1(\omega)$ [13, 18], mimicking pretty much precisely the overall trend of the measured optical conductivity (Figs. 1, 2, and 3).

The significance of orbital order is however controversial. For instance, Sugimoto et al. claim that at least below T_N the AFM ordering is enough to explain the discovered optical anisotropy, with no need to introduce any orbital order effect [19]. Valenzuela et al. [20] further point out that instead of orbital order, the anisotropy of the Fermi velocity, tightly related to the anisotropic topology of FS in a multi-orbital system, drives the anisotropy in the Drude weight and thus in the metallic part of the optical conductivity.

Our results could equally favor scenarios for the structural and magnetic transitions in the underdoped regime based on the ferro-orbital ordering or any models related to a spin-driven nematic order affecting however the charge channel of the excitation spectrum [9]. We nonetheless speculate that the orbital degree of freedom as well as its precursor effects above $T_{s,N}$ are indispensable ingredients at least in characterizing the normal state properties in the iron pnictides.

In conclusion, even though the multiband nature of the iron pnictides hampers precisely tracking the behavior of each single band crossing the Fermi level, our findings reveal a large anisotropy of the resulting conduction bands upon detwinning the specimen. This is reflected in the enhanced metallic (Drude) component of $\sigma_1(\omega)$ along the a axis with respect to the b axis, which progressively evolves with external stress upon lowering T. This has important implications with respect to the anisotropy of the dc transport properties, as elaborated elsewhere [11]. On the other hand, the optical dichroism at finite frequencies bears testimony to an electronic polarization accompanying the broken-symmetry orthorhombic (i.e., electronic nematic) phase or the induced orthorhombicity by the external symmetry breaking field (i.e., uniaxial stress) in the tetragonal phase, the latter imaging the impact of the nematic fluctuations into the electronic structure.

References

1. Fisher, I.R., Degiorgi, L., Shen, Z.X.: Rep. Prog. Phys **74**, 124506 (2011). and references therein
2. Tanatar, M.A., Kreyssig, A., Nandi, S., Ni, N., Bud'ko, S.L., Canfield, P.C., Goldman, A.I., Prozorov, R.: Phys. Rev. B **79**, 180508(R) (2009)
3. Chu, J.-H., Analytis, J.G., Press, D., De Greve, K., Ladd, T.D., Yamamoto, Y., Fisher, I.R.: Phys. Rev. B **81**, 214502 (2010)

4. Ruff, J.P.C., Chu, J.-H., Kuo, H.-H., Das, R.K., Nojiri, H., Fisher, I.R., Islam, Z.: Phys. Rev. Lett **109**, 027004 (2012)

5. Chu, J.-H., Kuo, H.-H., Analytis, J.G., Fisher, I.R.: Science **337**, 710 (2012)

6. Kuo, H.-H., Shapiro, M.C., Riggs, S.C., Fisher, I.R.: Phys. Rev. B **88**, 085113 (2013)

7. Kuo, H.-H., Fisher, I.R.: Phys. Rev. Lett **112**, 227001 (2014)

8. Mirri, C., Dusza, A., Bastelberger, S., Chu, J.-H., Kuo, H.-H., Fisher, I.R., Degiorgi, L.: Phys. Rev. B **89**, 060501(R) (2014). and Supplemental Material therein

9. Mirri, C., Dusza, A., Bastelberger, S., Chu, J.-H., Kuo, H.-H., Fisher, I.R., Degiorgi, L.: Phys. Rev. B **90**, 155125 (2014)

10. Dressel, M., Grüner, G.: Electrodynamics of Solids Cambridge University Press. Cambridge, England (2002)

11. Mirri, C., Dusza, A., Bastelberger, S., Chinotti, M., Chu, J.-H., Kuo, H.-H., Fisher, I.R., Degiorgi, L.: Phys. Rev. Lett. **115**, 107001 (2015)

12. Lucarelli, A., Dusza, A., Pfuner, F., Lerch, P., Analytis, J.G., Chu, J.-H., Fisher, I.R., Degiorgi, L.: New. J. Phys **12**, 073036 (2010)

13. Sanna, A., Bernardini, F., Profeta, G., Sharma, S., Dewhurst, J.K., Lucarelli, A., Degiorgi, L., Gross, E.K.U., Massidda, S.: Phys. Rev. B **83**, 054502 (2011)

14. Yin, Z.P., Haule, K., Kotliar, G.: Nat. Phys. **7**, 294 (2011)

15. Chen, C.-C., Maciejko, J., Sorini, A.P., Moritz, B., Singh, R.R.P., Devereaux, T.P.: Phys. Rev. B **82**, 100504(R) (2010)

16. Yi, M., Lu, D., Chu, J.-H., Analytis, J.G., Sorini, A.P., Kemper, A.F., Moritz, B., Mo, S.-K., Moore, R.G., Hashimoto, M., Lee, W.-S., Hussain, Z., Devereaux, T.P., Fisher, I.R., Shen, Z.-X.: PNAS **108**, 6878 (2011)

17. Yi, M., Lu, D.H., Moore, R.G., Kihou, K., Lee, C.-H., Iyo, A., Eisaki, H., Yoshida, T., Fujimori, A., Shen, Z.-X.: New. J. Phys **14**, 073019 (2012)

18. Lv, W., Phillips, P.: Phys. Rev. B **84**, 174512 (2011)

19. Sugimoto, K., Kaneshita, E., Tohyama, T.: J. Phys. Soc. Jap **80**, 033706 (2011)

20. Valenzuela, B., Bascones, E., Calderón, M.J.: Phys. Rev. Lett **105**, 207202 (2010)